Polarized spectral properties and laser demonstration of Nd-doped $Sr_3Y_2(BO_3)_4$ crystal

Zhongben Pan,[1] Haohai Yu,[1] Hengjiang Cong,[1] Huaijin Zhang,[1,*] Jiyang Wang,[1] Qing Wang,[2] Zhiyi Wei,[2] Zhiguo Zhang,[2] and R. I. Boughton[3]

[1]State Key Laboratory of Crystal Materials and Institute of Crystal Materials, Shandong University, Jinan 250100, China

[2]Institute of Physics, Chinese Academy of Sciences, Beijing 100190, China

[3]Department of Physics and Astronomy, Bowling Green State University, Bowling Green, Ohio 43403, USA

*Corresponding author: huaijnzhang@sdu.edu.cn

Received 22 June 2012; revised 13 September 2012; accepted 13 September 2012; posted 18 September 2012 (Doc. ID 171102); published 11 October 2012

Detailed polarized spectral properties of a 0.685 at. % Nd^{3+}:$Sr_3Y_2(BO_3)_4$ crystal grown by the Czochralski method have been investigated, including the absorption cross section, the emission cross section, and the fluorescence lifetime. The anisotropy of the spectral properties in different polarized directions was discussed thoroughly. The absorption and emission spectra of Nd^{3+} are found to be inhomogeneously broadened due to its internal disordered lattice. Additionally, the CW laser operation at 1.06 μm was also demonstrated for the first time. The maximum output power of 905 mW was achieved, with corresponding optical conversion efficiency of 10.8% and slope efficiency of 12.8%.

OCIS codes: 140.3380, 160.1190, 300.0300.

1. Introduction

Recently, the rapid development of ultrashort laser pulse technology has triggered great progress on the frontier of many fundamental sciences. It has now been found that ultrashort laser pulses have got wide applications in telemetry, microcosmic exploration, high-temperature plasma generation, etc. Therefore, many new ways to search for favorable solid-state laser materials have been explored to achieve efficient and compact high-energy ultrafast laser sources. Among these methods, disordered Nd^{3+}-doped crystals have attracted much attention as a new type of medium for ultrafast lasers at 1.06 μm. Compared to traditional Nd^{3+}-doped crystals, disordered host crystals will induce broad absorption and emission spectra due to their different crystal fields, which are caused by the random distribution of activator ions at the substitutional lattice sites. The broad absorption and fluorescence spectra of the disordered crystals thus favor efficient diode pumping and ultrashort pulse generation [1–4].

In this paper we focus on a new class of laser gain media with the general formula $M_3Re_2(BO_3)_4$, where M = Ca, Sr, or Ba and Re = Y, La, or Gd. In the past decades rare-earth-doped $M_3Re_2(BO_3)_4$ crystalline materials have attracted a great deal of research interest. Several members of rare-earth (Yb^{3+}, Nd^{3+}, Er^{3+})-doped $M_3Re_2(BO_3)_4$ (M = Ca, Sr, Ba; Re = Y, La, Gd) were investigated earlier [5–11], and the corresponding growth experiments showed that large-sized rare-earth-doped $M_3Re_2(BO_3)_4$ laser crystals can be grown well by using the Czochralski method, and the absorption and emission spectra are strongly inhomogeneously broadened due to the disordered lattice. The broad spectrum features a very efficient pumping and the production of ultrashort pulses [12,13].

$Sr_3Y_2(BO_3)_4$ belongs to the family of $M_3Re_2(BO_3)_4$ crystals, which crystallizes in the orthorhombic

1559-128X/12/307144-06$15.00/0

system with space group *P*nma. The unpolarized absorption and emission spectra of Nd^{3+}:$Sr_3Y_2(BO_3)_4$ were investigated before; the results show that Nd^{3+}:$Sr_3Y_2(BO_3)_4$ crystal is a potential laser material for diode laser pumping [5]. However, in those works the spectral information is limited by its unpolarized spectra and, most importantly, the laser performance has not been evaluated so far. Thus, in this work, a detailed polarized spectral measurement has been conducted and the laser demonstration of Nd^{3+}:$Sr_3Y_2(BO_3)_4$ crystal are reported for the first time, to our knowledge.

2. Experiment Procedure

A. Measurement of Effective Segregation Coefficients

The concentrations of elemental Nd, Sr, and Y in the crystal were measured using an x-ray fluorescence spectrometer (Primus II) with which the relative standard deviation is less than 1%. Based on the measurements, the effective segregation coefficients of elemental Nd, Sr, and Y in the crystal growth process were calculated. The measured sample, cut from the as-grown Nd^{3+}:$Sr_3Y_2(BO_3)_4$ crystal, was ground into powder for use in an x-ray fluorescence analysis apparatus (Primus II). The polycrystalline material used for growing the Nd^{3+}:$Sr_3Y_2(BO_3)_4$ crystal was employed as a comparison sample.

B. Spectral Measurement

A rectangular prism with dimensions of 5.44 mm × 6.30 mm × 7.00 mm ($a \times b \times c$) was cut from the as-grown crystal. All the surfaces of the sample were polished for the spectroscopy experiments. The polarization spectrum of the crystal was measured with incident light polarization parallel to the a, b, and c axes using a JASCO V-570 ultraviolet/visible/near-infrared (UV/Vis/NIR) spectrophotometer at room temperature over the wavelength range of 350–1000 nm. The fluorescence spectra from 850 to 1500 nm at room temperature and 77.3 K were recorded by a spectrofluorimeter (Edinburgh Instruments, FLS920). The excited source is a 450 W stable xenon lamp with a wavelength of 355 nm. The fluorescence decay curve at 1064 nm was measured with the same spectrofluorimeter, which was pumped by a 10 ns pulsed optical paremetric oscillator laser (Opolette 355 II) with a wavelength of 355 nm.

C. Laser Performance

With the laser sample cut along the b axis, CW laser operation was demonstrated by using a plano-concave resonator. The experimental laser setup is shown schematically in Fig. 1. The pump source was a fiber-coupled laser diode (LD) with the emission wavelength centered at 808 nm. The output beam of the LD was focused onto the Nd^{3+}:$Sr_3Y_2(BO_3)_4$ sample with a spot radius of about 0.2 mm and a numerical aperture of 0.22, achieved by using a focusing lens. The length between M1 and M2 is about 22 mm. M1 is a plane

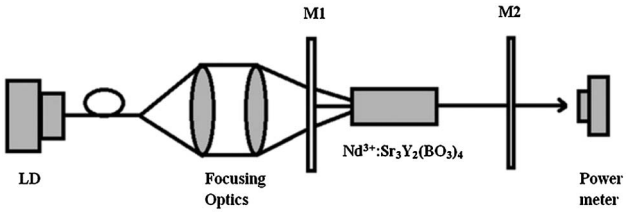

Fig. 1. Schematic diagram of the experimental laser setup.

mirror that is antireflection coated at 808 nm on the pump face, high reflectance coated at 1.06 μm, and high-transmittance coated at 808 nm on the other face. The output coupler M2 is a concave mirror with a radius of curvature of 200 mm, and the output transmission is 2.0% at 1.06 μm. The sample was cut to the dimensions 3 mm × 3 mm × 5 mm, and the 3 mm × 3 mm faces that are perpendicular to the b axis were polished. During the experiment, the crystal was wrapped with indium foil and mounted on a copper block cooled by water. The cooling water was maintained at a temperature of 6 °C.

3. Results and Discussion

A. Effective Segregation Coefficients

Table 1 shows the effective segregation coefficients of elemental Nd, Sr, and Y in the Nd^{3+}:$Sr_3Y_2(BO_3)_4$ crystal, which were calculated according to the following equation:

$$k_{\text{eff}} = \frac{c_1}{c_2}, \tag{1}$$

where c_1 and c_2 are the respective concentrations of the ions in the crystal and raw materials. From Table 1, it can be seen that the effective segregation coefficients of elemental Sr and Y in the Nd^{3+}:$Sr_3Y_2(BO_3)_4$ are close to 1 on the whole, which means that the elemental concentrations in the crystal are approximately equal to the elemental concentrations in the raw materials. Thus, the components of elemental Sr and Y in the Nd^{3+}:$Sr_3Y_2(BO_3)_4$ crystal growth process are uniform. The effective segregation coefficient of the Nd^{3+} ion in Nd^{3+}:$Sr_3Y_2(BO_3)_4$ is 1.375. It is higher than 1, which indicates that Nd^{3+} ions are comparatively easily doped into this crystal, and the Nd^{3+} ion concentration was determined to be 0.685 at. % (0.532×10^{20} ions/cm^3).

B. Spectroscopic Characteristics

The polarized absorption spectrum of the 0.685 at. % Nd^{3+}-doped $Sr_3Y_2(BO_3)_4$ crystal over the range of

Table 1. Effective Segregation Coefficients in $Sr_3Y_2(BO_3)_4$:Nd^{3+} Crystal

	Standard (wt %)	Sample (wt %)	K_{eff}
Nd	0.213	0.293	1.375
Sr	38.858	38.508	0.997
Y	26.154	25.021	0.957

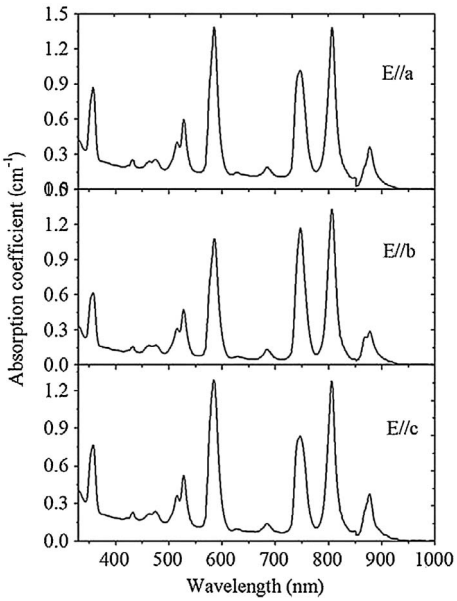

Fig. 2. Polarization absorption spectrum of Nd^{3+}:$Sr_3Y_2(BO_3)_4$.

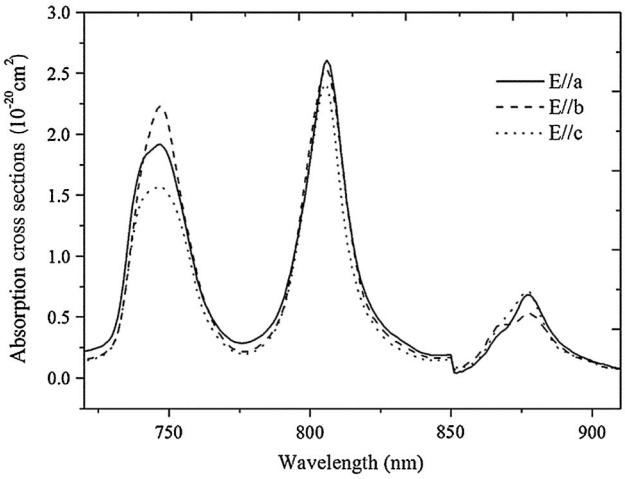

Fig. 3. Polarization absorption cross section of Nd^{3+}:$Sr_3Y_2(BO_3)_4$ over the range of 720–910 nm.

330–1000 nm is shown in Fig. 2. E represents the electric field of the incident light. Figure 3 shows an enlargement of the 720–910 nm region for clarity. Obviously, the polarization spectrum helps to gain a better understanding of the optical properties of Nd^{3+}:$Sr_3Y_2(BO_3)_4$ in contrast with the previously measured unpolarized spectrum. It can be seen from the two figures that the absorption spectrum shows a relatively strong directional dependence of the polarization due to the effect of anisotropy. From Fig. 3, it can be seen that the absorption is strong for $E\|a$ polarization, and the peak absorption cross section at 806 nm is about 2.605×10^{-20} cm^2 with a broad bandwidth (FWHM) of about 16 nm. For the $E\|b$ and $E\|c$ polarizations, the maximum absorption cross sections near 805 nm are 2.531×10^{-20} cm^2 and 2.394×10^{-20} cm^2 and the bandwidths (FWHM) are 17 and 16 nm, respectively. The wide bandwidth signifies that Nd^{3+}:$Sr_3Y_2(BO_3)_4$ is quite suitable for diode pumping and indicates inhomogeneous broadening behavior [14], which is probably due to the structural disorder of the crystal.

The Judd–Ofelt (J–O) theory is applied to analyze the room temperature absorption spectra [15,16], since the J–O theory and its extension have become the most widely used method for the analysis of spectroscopic properties of rare-earth-ion-doped crystals and glasses. Thus, only the calculational results are presented; the detailed calculation procedure is similar to that reported in [1]. The reduced matrix element of the unit tensor operators used in the fitting can be found in [17]. The refractive index used for the calculation was taken to be roughly 1.74 [5]. The measured transition-line intensity and oscillator strength, denoted by S_{exp} and P_{exp}, respectively, are listed in Table 2. The calculated J–O intensity parameters Ω_t ($t = 2, 4, 6$) are listed in Table 3. For a biaxial crystal, the effective J–O intensity parameters are defined as in [18], and their values are also listed in Table 3. Table 4 shows the Ω_t ($t = 2$, 4 and 6) values for Nd^{3+}:$Sr_3Y_2(BO_3)_4$ obtained in this work and makes a comparison with the same parameters for other Nd-doped crystals [1,19–22]. It is known that the value of the intensity parameter Ω_2 depends on the structure and the coordination symmetry of a crystal. Generally, the higher the value of Ω_2, the larger the fraction of covalent bonding the compound

Table 2. Experimental Transition-Line Intensity Parameters and Oscillator Strengths of the Polarization Absorption Spectrum of Nd^{3+}:$Sr_3Y_2(BO_3)_4$

	$E\|a$		$E\|b$		$E\|c$	
Transition Final State $4f^n\psi' J'$	$S_{exp}(J \to J')$ (10^{-20} cm^2)	$P_{exp}(J \to J')$ (10^{-6})	$S_{exp}(J \to J')$ (10^{-20} cm^2	$P_{exp}(J \to J')$ (10^{-6})	$S_{exp}(J \to J')$ (10^{-20} cm^2	$P_{exp}(J \to J')$ (10^{-6})
$^4D_{1/2}$	2.51	12.31	2.11	9.71	2.26	10.38
$^4P_{1/2}$	0.19	0.77	0.15	0.55	0.16	0.61
$^4G_{11/2}$	0.56	2.07	0.57	1.96	0.49	1.69
$^4G_{9/2}$	2.06	6.84	2.04	6.37	2.19	6.82
$^4G_{5/2}$	4.87	14.56	4.50	12.61	5.29	14.84
$^4F_{9/2}$	0.25	0.64	0.28	0.67	0.25	0.60
$^4S_{3/2}$	3.38	7.93	3.93	8.63	3.15	6.91
$^4H_{9/2}$	3.64	7.90	3.88	7.90	3.52	7.18
$^4F_{3/2}$	1.05	2.10	0.93	1.73	1.08	2.03

Table 3. Judd–Ofelt Intensity Parameters of Nd^{3+} in $Sr_3Y_2(BO_3)_4$

Intensity Parameters ($\Omega \times 10^{-20}$ cm^2)	$E\|a$	$E\|b$	$E\|c$	Effective
Ω_2	2.21	2.31	2.89	2.47
Ω_4	5.48	4.25	5.04	4.92
Ω_6	6.28	7.72	5.80	6.60

contains; that is, if the crystal has a relatively high value of Ω_2, the crystal may exhibit a glasslike behavior. We believe that the high Ω_2 parameter is one of the possible factors that can prove the glassy behavior of the materials. From Table 4 one can conclude that Nd^{3+}:$Sr_3Y_2(BO_3)_4$ has a large fraction of covalent bonding because of the high Ω_2 value [8,23]. In addition, the thermal conductivity of Nd^{3+}:$Sr_3Y_2(BO_3)_4$ was measured in our group, and similar to Nd^{3+}:$Gd_3Ca_2(BO_3)_4$, it increases with increasing temperature, which indicates a glasslike behavior [8]. Thus, considering the two behaviors shown above, we can further conclude that Nd^{3+}:$Sr_3Y_2(BO_3)_4$ indeed exhibits a glasslike behavior, which conforms to the disordered structure of the crystal. In addition, we know that the value of the parameter Ω_2 has no practical effect on the emission properties of the crystal from the $^4F_{3/2}$ state, as they mainly depend on the Ω_4 and Ω_6 parameters. The spectroscopic quality parameter $X = \Omega_4/\Omega_6$ is 0.75 is less than 1 and thus indicates that emission to the $^4I_{9/2}$ manifold is more feasible than to the $^4I_{9/2}$ manifold.

Using the calculated J–O intensity parameters, the radiative transition rate $A_{(J''\to J')}$ and fluorescence branching ratio $\beta_{J''J}$ of Nd^{3+}:$Sr_3Y_2(BO_3)_4$ are calculated, and the results along the three polarization directions are listed in Table 5.

The radiative lifetime $\tau_{\rm rad}$ of the $^4F_{3/2}$ manifold is the reciprocal of the total spontaneous emission probability from the manifold. For an anisotropic crystal, the total spontaneous emission probability is given as

$$A_{\rm Total}(J'') = \frac{\sum_q \sum_{J'} A(J'' \to J')}{3}. \quad (2)$$

So, the radiative lifetime of the $^4F_{3/2}$ manifold for Nd^{3+} in $Sr_3Y_2(BO_3)_4$ is estimated to be 208.17 μs. The fluorescence decay curve of $^4F_{3/2}$ is shown in Fig. 4. By linear fitting, the fluorescence lifetime is found to be 75.8 μs, so the radiative quantum efficiency of the $^4F_{3/2}$ manifold is about $\eta = 75.8/208.17 = 36.41\%$. We noticed that the fluorescence lifetime measured in our paper is significantly longer than that published in [5]. We believe that the fluorescence lifetime decreases when the concentration of Nd^{3+} ions increases because of the concentration quenching of Nd^{3+}.

The stimulated emission cross section σ_e can be estimated from the measured fluorescence spectrum by the Füchtbauer–Ladenburg method:

$$\sigma_e(\lambda) = \frac{\lambda^5 A(J'' \to J') I(\lambda)}{8\pi c n^2 \int \lambda I(\lambda) d\lambda}, \quad (3)$$

where $I(\lambda)$ is the fluorescence intensity at wavelength λ and n is the refractive index, which was taken to be roughly 1.74 [5]. The room temperature and low temperature (77.2 K) fluorescence spectra are shown in Fig. 5, and the emission cross-section values at the peak fluorescence wavelength are listed in Table 5. The peak wavelength in the room temperature fluorescence spectrum for $E\|c$ is located at 1064 nm and differs from the values obtained for $E\|a$ and $E\|b$, which are shifted to 1063 nm, even though the FWHM at peak wavelength for the different polarization directions has the same value of 30 nm. Additionally, compared with the room temperature fluorescence spectra, the value of FWHM at 1063 nm in the 77.2 K unpolarized spectrum is 29 nm, showing a very small change. The broad bandwidth is similar to Nd:glass (20–30 nm), which can support pulses of less than 100 fs [24,25]. Thus, such a large bandwidth shows that

Table 4. Comparison of Judd–Ofelt Parameters for Nd^{3+}:$Sr_3Y_2(BO_3)_4$ with Other Nd-Doped Crystals

Crystals	$\Omega_2 \times 10^{-20}$ cm^2	$\Omega_4 \times 10^{-20}$ cm^2	$\Omega_6 \times 10^{-20}$ cm^2	X	Reference
Nd^{3+}:$Sr_3Y_2(BO_3)_4$	2.47	4.92	6.60	0.75	(This work)
Nd^{3+}:$SrGdGa_3O_7$	1.88 ~ 2.94	4.44 ~ 6.33	2.96 ~ 6.96	0.91 ~ 1.5	[1,19]
Nd^{3+}:YAG	0 ~ 0.37	2.29 ~ 3.2	4.6 ~ 5.97	0.38 ~ 0.70	[20–22]
Nd^{3+}:GGG	0 ~ 0.02	3.3 ~ 6.7	3.7 ~ 6.7	0.89 ~ 1	[20,22]

Table 5. Luminescence Parameters of Nd^{3+}:$Sr_3Y_2(BO_3)_4$ for the Radiative $^4F_{3/2} \to {}^4I_{J'}$ Transition

	$E\|a$				$E\|b$				$E\|c$			
Final State	$S_{\rm cal}(J''\to J')$ (10^{-20} cm^2)	$A(J''\to J')$ (s^{-1})	$\beta_{J''J}$ (%)	$\sigma_e(\lambda)$ (10^{-20} cm^2)	$S_{\rm cal}(J''\to J')$ (10^{-20} cm^2)	$A(J''\to J')$ (s^{-1})	$\beta_{J''J}$ (%)	$\sigma_e(\lambda)$ (10^{-20} cm^2)	$S_{\rm cal}(J''\to J')$ (10^{-20} cm^2)	$A(J''\to J')$ (s^{-1})	$\beta_{J''J}$ (%)	$\sigma_e(\lambda)$ (10^{-20} cm^2)
$^4I_{9/2}$	1.61	1903.56	39.05	0.25	1.41	1659.24	32.86	0.31	1.48	1752.32	39.06	0.32
$^4I_{11/2}$	3.33	2453.69	50.33	2.98	3.75	2756.47	54.59	3.46	3.08	2257.56	50.32	2.87
$^4I_{13/2}$	1.33	494.64	10.15	1.01	1.64	605.34	11.99	1.21	1.23	454.79	10.14	0.93
$^4I_{15/2}$	0.18	23.39	0.48		0.22	28.76	0.57		0.16	21.60	0.48	

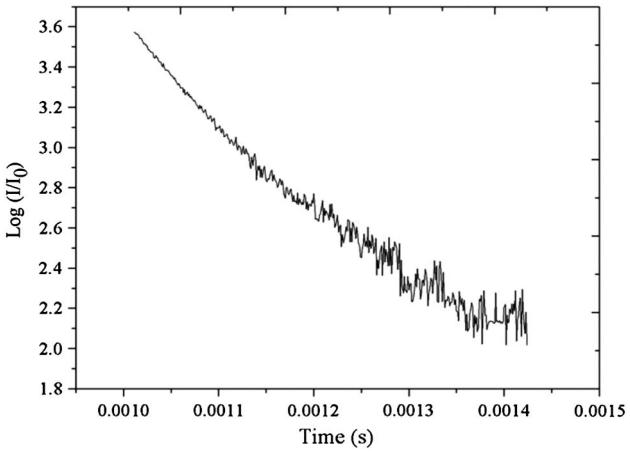

Fig. 4. Fluorescence decay curve of Nd^{3+}:$Sr_3Y_2(BO_3)_4$.

Nd^{3+}:$Sr_3Y_2(BO_3)_4$ may also possibly be used in laser systems to produce femtosecond pulses [26]. It can be concluded that the broad room temperature absorption and emission bands together with the 77.2 K fluorescence spectrum show an inhomogeneous broadening behavior of the Nd^{3+}:$Sr_3Y_2(BO_3)_4$ crystal. Generally, the major broadening mechanisms at room temperature are homogeneous broadening from the thermal vibration of the lattice and inhomogeneous broadening from a disordered crystal lattice. While at a low temperature, the inhomogeneous broadening dominates due to the weakening of lattice vibration. Here we can find that the inhomogeneous broadening behavior plays a decisive role, not only at room temperature, but also at low temperatures. We know that Nd^{3+}:$Sr_3Y_2(BO_3)_4$ crystal is a homology of Nd^{3+}:$Ca_3Gd_2(BO_3)_4$, and the inhomogeneous broadening behavior in the Nd^{3+}:$Ca_3Gd_2(BO_3)_4$ crystal has been discussed in our previous paper [8]. Thus, we believe that the inhomogeneous broadening of the Nd^{3+} lines is also attributed to the variation of the local crystal field surrounding the Nd^{3+} ions resulting from the high degree of structural disorder, in that Nd^{3+}, Sr^{2+},

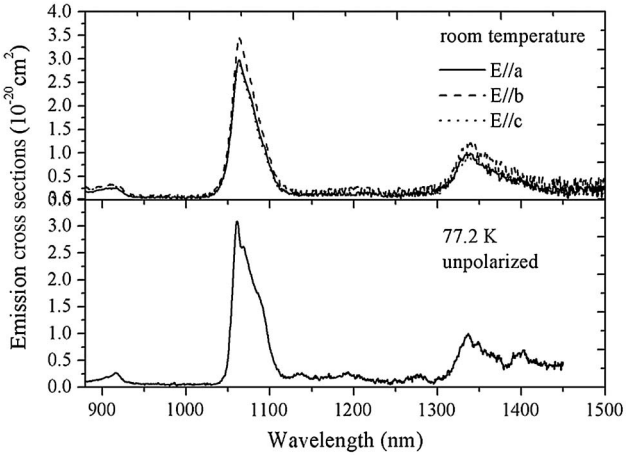

Fig. 5. Fluorescence spectra of Nd^{3+}:$Sr_3Y_2(BO_3)_4$: (a) room temperature polarized emission cross sections and (b) 77.2 K unpolarized emission cross section.

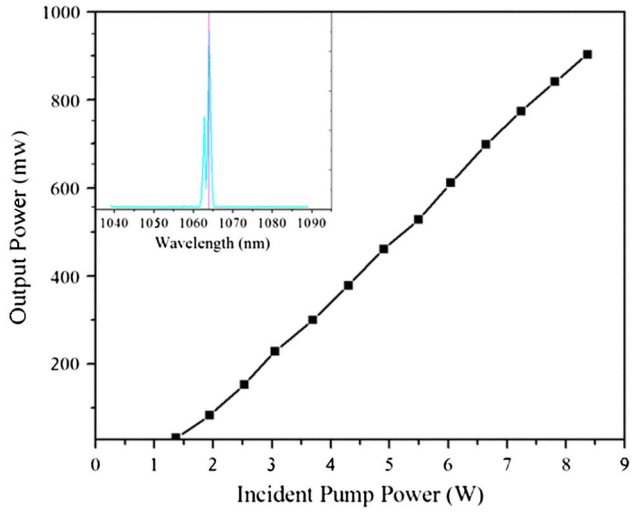

Fig. 6. (Color online) Average output power versus incident pump power. Inset: Spectrum of Nd^{3+}:$Sr_3Y_2(BO_3)_4$.

and Y^{3+} ions are randomly situated at three different symmetry sites in the Nd^{3+}:$Sr_3Y_2(BO_3)_4$ structure. In addition, from Table 5, the emission cross-section values for the three polarization directions at 1.06 μm are 2.98×10^{-20} cm^2, 3.46×10^{-20} cm^2, and 2.87×10^{-20} cm^2, respectively. Though the emission cross-section values of Nd^{3+}:$Sr_3Y_2(BO_3)_4$ are relatively smaller than other Nd-doped crystals, we still believe that Nd^{3+}:$Sr_3Y_2(BO_3)_4$ is a good candidate as a laser medium, especially in the femtosecond pulse field because of its very broad emission band.

C. Laser Performance

CW laser performance at 1.06 mm was demonstrated for the first time (to our knowledge). The output power under various incident power values was measured using a power meter, and the results are shown in Fig. 6. The pump threshold of Nd^{3+}:$Sr_3Y_2(BO_3)_4$ is 1.35 W, and a maximum output power of 905 mW at 1.06 μm was achieved at a pump power of 8.36 W. An optical-to-optical conversion efficiency of 10.8% and a slope efficiency of 12.8% were derived from the linear part of the curve. It can be seen in Fig. 6 that the output power is not saturated when the incident power is 8.36 W, so higher output power may be achieved when the pump power is increased. In addition, the sample used in the laser experiment was not coated, and only one output coupling with 2.0% transmission was used in the experiment. Therefore, more efficient laser output can be realized if the sample and the transmission output coupling are optimized. With a spectrum analyzer, the emission spectrum was recorded and is shown in the upper left of Fig. 6. From Fig. 6, it can be seen that the laser band is centered at 1064 nm.

4. Conclusions

A large-sized and high-quality Nd^{3+}:$Sr_3Y_2(BO_3)_4$ crystal was grown by the Czochralski method. The complete set of spectral and laser performance has been characterized in detail. The effective

segregation coefficient of Nd^{3+} was determined to be 1.375, which indicates that Nd^{3+} ions are comparatively easily doped into this crystal. The polarized absorption spectra, fluorescence spectra, and decay curve of Nd^{3+}:$Sr_3Y_2(BO_3)_4$ were measured. The results show that the absorption and emission spectra of Nd^{3+} have been inhomogeneously broadened, which is attributed to its inner disordered structure. For suitability as a match to LD pumping, the width of the absorption band around 808 nm is about 16 nm. The broad emission spectrum (FWHM = 30 nm) shows that Nd^{3+}:$Sr_3Y_2(BO_3)_4$ can potentially be used to yield femtosecond laser pulses. From the J–O theory, the spectral parameters along different polarization directions were also calculated, showing anisotropic behavior. The radiative lifetime of the $^4F_{3/2}$ manifold for Nd^{3+} in $Sr_3Y_2(BO_3)_4$ is estimated to be 208.17 μs. From the fluorescence decay curve, the fluorescence lifetime is found to be 75.8 μs, giving a radiative quantum efficiency of about $\eta = 75.8/208.17 = 36.41\%$. The laser operation under LD end pumping at 1.06 μm was demonstrated for the first time, to our knowledge. A maximum power of 905 mW was obtained with an optical conversion efficiency of 10.8% and slope efficiency of 12.8%. Therefore, all of these properties show that Nd^{3+}:$Sr_3Y_2(BO_3)_4$ is a very promising crystalline laser material.

This work was supported by the National Natural Science Foundation of China (Grant Nos. 51025210 and 51021062), the National Basic Research Program of China (Grant No. 2010CB630702), and the Program of Introducing Talents of Discipline to Universities in China (111 program).

References

1. Y. Y. Zhang, H. J. Zhang, H. H. Yu, J. Y. Wang, W. L. Gao, M. Xu, S. Q. Sun, M. H. Jiang, and R. I. Boughton, "Synthesis, growth, and characterization of Nd-doped $SrGdGa_3O_7$ crystal," J. Appl. Phys. **108**, 063534 (2010).
2. T. T. Basiev, N. A. Es'kov, A. Ya. Karasik, V. V. Osiko, A. A. Sobol, S. N. Ushakov, and M. Helbig, "Disordered garnets $Ca_3(Nb, Ga)_5O_{12}$:Nd^{3+}-prospective crystals for powerful ultrashort-pulse generation," Opt. Lett. **17**, 201–203 (1992).
3. G. Q. Xie, D. Y. Tang, W. D. Tan, H. Luo, H. J. Zhang, H. H. Yu, and J. Y. Wang, "Subpicosecond pulse generation from a Nd: CLNGG disordered crystal laser," Opt. Lett. **34**, 103–105 (2009).
4. G. Q. Xie, D. Y. Tang, H. Luo, H. J. Zhang, H. H. Yu, J. Y. Wang, X. T. Tao, M. H. Jiang, and L. J. Qian, "Dual-wavelength synchronously mode-locked Nd:CNGG laser," Opt. Lett. **33**, 1872–1874 (2008).
5. Y. Zhang, Z. B. Lin, Z. S. Hu, and G. F. Wang, "Growth and spectroscopic properties of Nd^{3+}-doped $Sr_3Y_2(BO_3)_4$ crystal," J. Solid State Chem. **177**, 3183–3186 (2004).
6. B. V. Mill, A. M. Tkachuk, E. L. Belokoneva, G. I. Ershova, D. I. Mironov, and I. K. Razumova, "Spectroscopic studies of $Ln_2Ca_3B_4O_{12}$-Nd^{3+} (Ln = Y, La, Gd) crystals," J. Alloys Compd. **275–277**, 291–294 (1998).
7. Y. Wang, C. Y. Tu, Z. Y. You, J. F. Li, Z. J. Zhu, G. H. Jia, X. A. Lu, and B. C. Wu, "Optical spectroscopy of $Ca_3Gd_2(BO_3)_4$:Nd^{3+} laser crystal," J. Mod. Opt. **53**, 1141–1148 (2006).
8. Z. B. Pan, H. J. Zhang, H. H. Yu, M. Xu, Y. Y. Zhang, S. Q. Sun, J. Y. Wang, Q. Wang, Z. Y. Wei, and Z. G. Zhang, "Growth and characterization of Nd-doped disordered $Ca_3Gd_2(BO_3)_4$ crystal," Appl. Phys. B **106**, 197–209 (2012).
9. P. Ma, J. T. Chen, Z. S. Hu, Z. B. Lin, and G. F. Wang, "Structure of $Ba_3Y_2(BO_3)_4$ crystal," Mater. Res. Innovations **9**, 63–64 (2005).
10. C. Y. Tu, Y. Wang, Z. Y. You, J. F. Li, Z. J. Zhu, and B. C. Wu, "Growth and spectroscopic characteristics of $Ca_3Gd_2(BO_3)_4$:Yb^{3+} laser crystal," J. Cryst. Growth **265**, 154–158 (2004).
11. A. Brenier, C. Y. Tu, Y. Wang, Z. Y. You, Z. J. Zhu, and J. F. Li, "Diode-pumped laser operation of Yb^{3+}-doped $Y_2Ca_3B_4O_{12}$ crystal," J. Appl. Phys. **104**, 013102 (2008).
12. Z. Burshtein, Y. Shimony, I. Levy, A. M. Lejus, J. M. Benitez, and F. Mougel, "Refractive-index studies in $Ca_2Ga_2SiO_7$ and $SrLaGa_3O_7$ melilite-type compounds," J. Opt. Soc. Am. B **13**, 1941–1944 (1996).
13. A. V. Terentiev, P. V. Prokoshin, K. V. Yumashev, V. P. Mikhailov, W. Ryba-Romanowski, S. Golab, and W. Pisarski, "Passive mode locking of a Nd^{3+}:$SrLaGa_3O_7$ laser," Appl. Phys. Lett. **67**, 2442–2444 (1995).
14. W. F. Krupke, "Optical absorption and fluorescence intensities in several rare-earth-doped Y_2O_3 and LaF_3 single crystals," Phys. Rev. **145**, 325–337 (1966).
15. B. R. Judd, "Optical absorption intensities of rare-earth ions," Phys. Rev. **127**, 750–761 (1962).
16. G. S. Ofelt, "Intensities of crystal spectra of rare-earth ions," J. Chem. Phys. **37**, 511–520 (1962).
17. W. T. Carnall, P. R. Fields, and K. Rajnak, "Electronic energy levels in the trivalent lanthanide aquo ions. I. Pr^{3+}, Nd^{3+}, Pm^{3+}, Sm^{3+}, Dy^{3+}, Ho^{3+}, Er^{3+}, and Tm^{3+}," J. Chem. Phys. **49**, 4424–4442 (1968).
18. Z. Luo, X. Chen, and T. Zhao, "Judd-Ofelt parameter analysis of rare earth anisotropic crystals by three perpendicular unpolarized absorption measurements," Opt. Commun. **134**, 415–422 (1997).
19. F. Hanson, D. Dick, H. R. Verdun, and M. Kokta, "Optical properties and lasing of Nd:$SrGdGa_3O_7$," J. Opt. Soc. Am. B **8**, 1668–1673 (1991).
20. E. Cavalli, E. Zannoni, A. Belletti, V. Carozzo, A. Toncelli, M. Tonelli, and M. Bettinelli, "Spectroscopic analysis and laser parameters of Nd^{3+} in $Ca_3Sc_2Ge_3O_{12}$ garnet crystals," Appl. Phys. B **68**, 677–681 (1999).
21. Y. Guyot, H. Manaa, J. Y. Rivoire, R. Moncorgé, N. Garnier, E. Descroix, M. Bon, and P. Laporte, "Excited-state-absorption and upconversion studies of Nd^{3+}-doped single crystals $Y_3A_{15}O_{12}$, $YLiF_4$, and $LaMgA_{11}O_{19}$," Phys. Rev. B **51**, 784–799 (1995).
22. A. A. Kaminskii, *Crystalline Lasers: Physical Processes and Operating Schemes* (CRC Press, 1996), pp. 231–238.
23. Y. Wang, C. Y. Tu, Z. Y. You, J. F. Li, Z. J. Zhu, G. H. Jia, X. A. Lu, and B. C. Wu, "Optical spectroscopy of $Ca_3Gd_2(BO_3)_4$:Nd^{3+} laser crystal," J. Mod. Opt. **53**, 1141–1148 (2006).
24. C. Spielmann, F. Krausz, T. Brabec, E. Wintner, and A. Schmidt, "Femtosecond passive mode locking of a solid-state laser by a dispersively balanced nonlinear interferometer," Appl. Phys. Lett. **58**, 2470–2472 (1991).
25. D. Kopf, F. X. Kärtner, U. Keller, and K. J. Weingarten, "Diode-pumped mode-locked Nd:glass lasers with an antiresonant Fabry–Perot saturable absorber," Opt. Lett. **20**, 1169–1171 (1995).
26. A. A. Kaminskii, *Laser Crystals* (Springer-Verlag, 1981), pp 12–27.